

Nonlinearity-controllable all-optical logic gates based on broadband defect mode

BIN LIU, HUIPING TIAN, HUI LU, YUEFENG JI*

Key Laboratory of Information Photonics and Optical Communications,
Beijing University of Posts and Telecommunications, Ministry of Education,
Beijing 100876, China

*Corresponding author: jyf@bupt.edu.cn

To avoid the adverse effect of unstable nonlinear progress on the design of all-optical logic gates, the broadband defect mode of one-dimensional photonic crystal with dual-defects has been studied. By using transfer matrix method, influences of period number and refractive indices on crystal's transmission spectrum are analyzed. It is pointed out that with proper parameters, broadband defect mode, which could be used to reduce the influence between the nonlinear refractive index and field distribution, can be gained. Due to this fact, the designed XOR, AND and NOT logic gates can be steadily controlled with low-threshold and high-contrast.

Keywords: photonic crystals, all-optical logic gates, broadband defect mode, nonlinearity.

1. Introduction

As one of the key components to realize all optical networks [1], all-optical logic gates (AOLG) have attracted extensive attention for their important applications in optical computing, clock recovery, optical buffering and signal regeneration. Recently, several solutions [2–6] have been proposed to realize AOLG, but there are still many disadvantages in those proposals. For example, AOLG based on nonlinear fiber [2] are difficult to be miniaturized and integrated, while the spontaneous emission noise is harmful for the ones based on semi-conductor optical amplifier [3]. Considered that devices based on photonic crystals (PC) [7, 8] are universally spontaneous emission suppressing, small in size and easy to be integrated, AOLG based on PC [9–12] become another research hot-spot in related fields at present.

Compared to two-dimensional or three-dimensional PC, one-dimensional (1D) PC are studied more sufficiently and maturely. Furthermore, the fabrication of 1D PC has the advantages of simple design, low cost and high precision, thus achievement in the research of AOLG was firstly gained based on 1D PC [9–11]. The basic principle is that PC's band-gap position could be dynamically shifted due to the changing of nonlinear refractive index according to the light intensity. But there are two key problems in that process. One is that the requirements for the nonlinear coefficient of

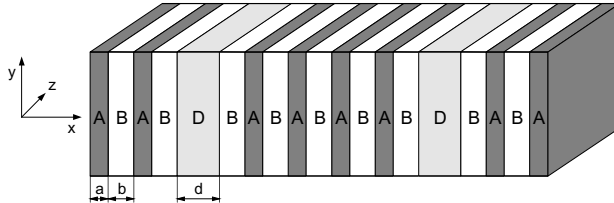


Fig. 1. Structure of 1D PC with dual-defects.

material and the intensity of input light are too high to be satisfied. The other one is that the nonlinear process is unstable. Previous studies did not solve those two problems, especially the latter one. In this letter, by simulating the transmission spectrum and field distribution of 1D PC, we propose a solution that uses light localization in the nonlinear defect layer to enhance the nonlinearity of PC, and realizes stable control of light intensity on the nonlinear refractive index with broadband defect mode (BDM) introduced by dual-defects. On those bases, we design AOLG such as XOR, AND and NOT.

2. Theoretical model

As a model of AOLG, we consider the 1D PC with dual-defects, which is formed by alternately stacking two dielectrics A and B along the x -direction with two defects D, and whose structure can be described as $(AB)^S D (BA)^N B (AB)^N D (BA)^S$. The refractive indices of A, B, D are n_a , n_b and n_d , respectively, while their geometrical thicknesses are respectively a , b and d . S and N are the period numbers of the AB or BA unit. Figure 1 shows the structure of 1D PC when S and N are equal to 2.

Transfer matrix method [13] is used for numerical simulation of such 1D PC. Electromagnetic field in the k -th layer, which is a dual vector, can be expressed as:

$$\Phi_k(x) = \begin{bmatrix} E_k(x) \\ i c B_k(x) \end{bmatrix} \quad (1)$$

If a vertical light is incident in the layer, with Maxwell equations, Eq. (1) could be changed as [14]:

$$\Phi_k(x_{k-1} + \Delta x) = \left[M_k(\Delta x) M_{k-1}(d_{k-1}) \dots M_1(d_1) \right] \Phi(x_0) \quad (2)$$

where

$$M_k(\Delta x) = \begin{bmatrix} \cos\left(\frac{\omega}{c} n_k \Delta x\right) & -n_k^{-1} \sin\left(\frac{\omega}{c} n_k \Delta x\right) \\ -n_k \sin\left(\frac{\omega}{c} n_k \Delta x\right) & \cos\left(\frac{\omega}{c} n_k \Delta x\right) \end{bmatrix} \quad (3)$$

In the two equations above, x_{k-1} is the distance to the left interface of the k -th layer; d_k and n_k are the thickness and refractive index of the k -th layer, respectively; ω is the frequency of the input light; c is the speed of light in a vacuum. According to Eq. (2), the electromagnetic field at the exit facet ($x = x_{4S+4N+3}$) could be written as:

$$\begin{aligned}\Phi(x_{4S+4N+3}) &= \left[M_{4S+4N+3}(d_{4S+4N+3})M_{4S+4N+2}(d_{4S+4N+2})\dots M_1(d_1) \right] \Phi(x_0) \\ &= \begin{bmatrix} M_{11} & M_{12} \\ M_{21} & M_{22} \end{bmatrix} \Phi(x_0)\end{aligned}\quad (4)$$

Thus the reflection coefficient r and transmission coefficient t of the electric field in PC can be described as:

$$r = \frac{E_r(x_0)}{E_i(x_0)} = \frac{M_{22} - M_{11} - i(M_{12} + M_{21})}{M_{22} + M_{11} - i(M_{12} - M_{21})} \quad (5)$$

$$t = \frac{E_t(x_{4S+4N+3})}{E_i(x_0)} = \frac{2}{M_{22} + M_{11} - i(M_{12} - M_{21})} \quad (6)$$

while the reflectivity R and transmittance T are given by:

$$R = r \cdot r^* \quad (7)$$

$$T = t \cdot t^* \quad (8)$$

The field distribution of PC can be calculated by Eq. (1), while the PC's transmission spectrum can be obtained by Eq. (8).

3. Results and discussion

3.1. Realization of BDM in 1D PC with dual-defects

As it is known, the introduction of a defect into 1D PC will lead to a narrow transmission peak, which is called defect mode, appearing in the band-gap. Further studies have concluded that when we introduced multi-defects, the number of the transmission peaks will be more than one. It is hoped that BDM can be realized by tuning the structure and material parameters of 1D PC with multi-defects. Take the one with dual-defects for example, as shown in Fig. 1, the effect of period number on transmission spectrum is analyzed firstly.

The refractive indices of A, B and D are assumed to be $n_a = 2.5$, $n_b = 1.5$, and $n_d = 3.5$, respectively. The optical thicknesses of A and B are both quarter-wavelength, while the one of D is half-wavelength, that is $a n_a = b n_b = \lambda_0/4$, $d n_d = \lambda_0/2$, where λ_0 is the central wavelength assumed to be 1550 nm, and the central frequency is ω_0

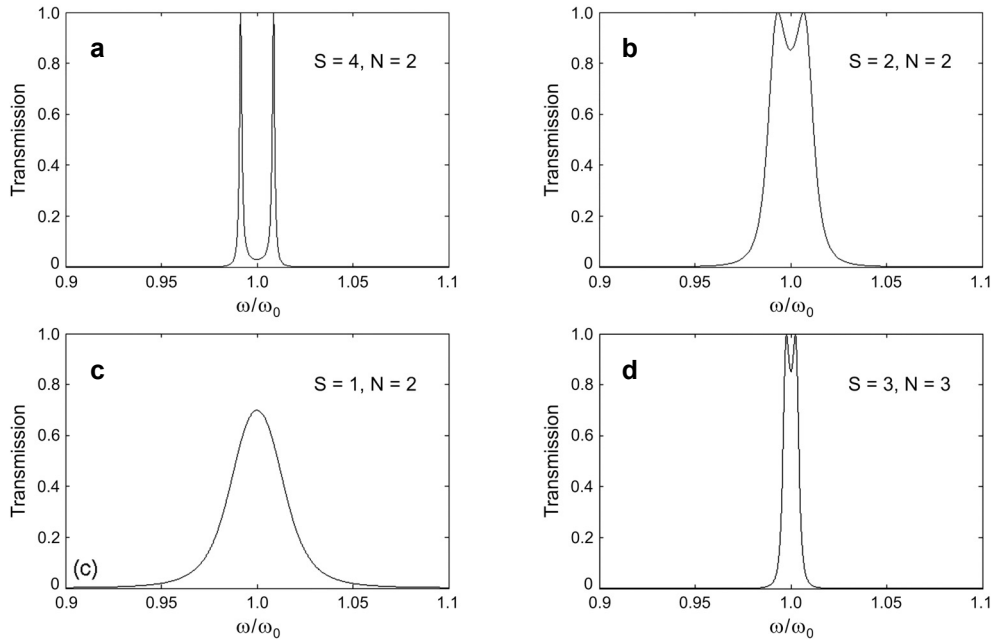


Fig. 2. Effects of period number on transmission spectrum of 1D PC with dual-defects.

accordingly. In this letter, all the lights are considered to be normally incident upon the surface of the PC. Under the above-mentioned conditions, the effect of period number on transmission spectrum of PC is shown in Fig. 2. The horizontal axis represents the normalized frequency of the input light, and the vertical axis represents the transmittance of PC. Because the defect modes near the central frequency are what we are interested in, the range of horizontal axis is chosen from 0.9 to 1.1.

As can be seen in Fig. 2a, there are two defect modes in the transmission spectrum of 1D PC with dual-defects. These modes become closer to each other until their overlapping with the decreasing S/N ; when S/N decreases to 1, BDM is basically formed, as shown in Fig. 2b; Fig. 2c indicates that the peak value of BDM will decrease with further reduction of S/N ; and it can be concluded that in the condition of $S/N = 1$, the enlargement of S and N will lead to the narrowing of BDM by comparing Fig. 2d with Fig. 2b.

The effect of material refractive indices on transmission spectrum of 1D PC with dual-defects is studied secondly.

Assume that $S = N = 2$, when the other parameters are the same as the ones in Fig. 2, the effects of refractive indices of A, B and D on PC's transmission spectrum are shown in Fig. 3. Figure 3a shows that the broadband transmission peak will become narrow with the increasing n_a , and the transmittance at central frequency maintains constant; Figure 3b indicates that the broadband transmission peak will become narrow with the decreasing n_b too, but the transmittance at central frequency becomes larger. It can be seen in Fig. 3c that when the optical thickness of the defect layer

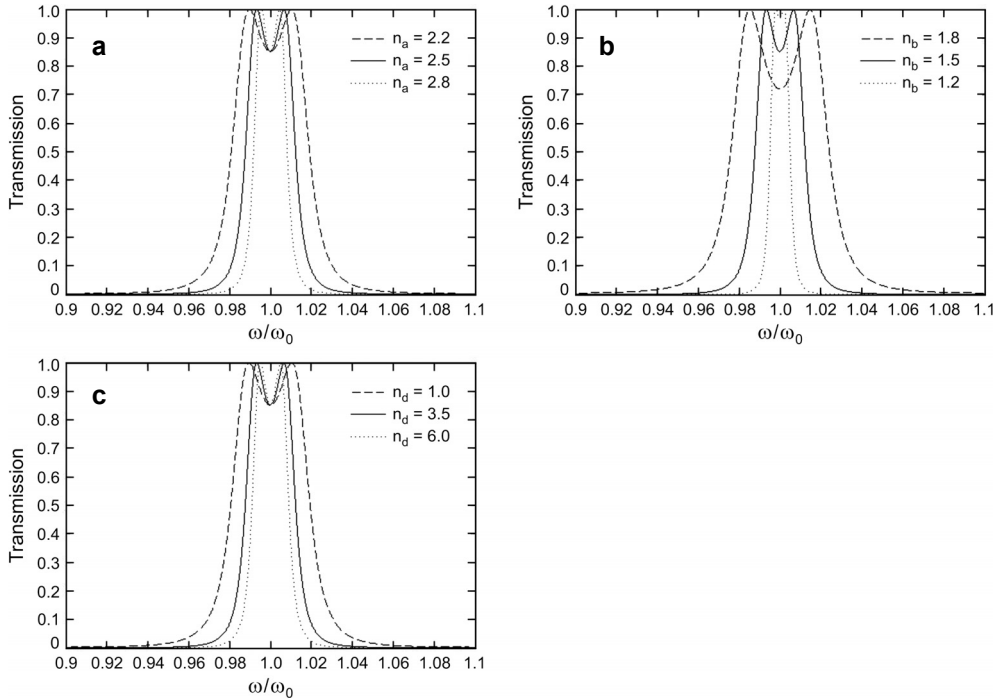


Fig. 3. Effects of material refractive indices on transmission spectrum of 1D PC with dual-defects, (a), (b), and (c) are corresponding to n_a , n_b , and n_d , respectively.

keeps as half-wavelength, the broadband transmission peak becomes narrow with the increasing n_d , and the transmittance at central frequency maintains constant.

According to the above results, we can realize flattened and completely transmitting BDM with proper period number and material refractive indices in 1D PC with the structure of $(AB)^S D(BA)^N B(AB)^N D(BA)^S$. Assuming that $S=N=1$, $n_a=1.5$, $n_b=1.0$, $n_d=3.5$, such BDM is shown in Fig. 4. It can be used for a broadband filter. AOLG discussed in this letter and other applications are based on nonlinear 1D PC.

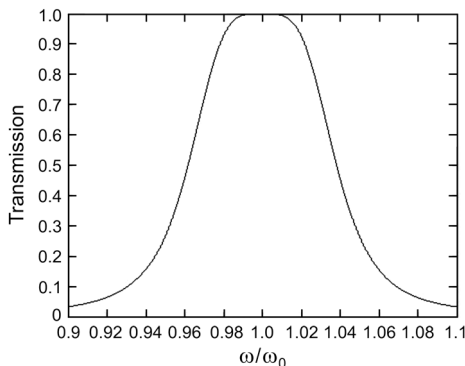


Fig. 4. BDM of 1D PC with dual-defects.

3.2. Field distribution of 1D PC with dual-defects

In 1D PC with dual-defects, input light with the frequency of ω_0 will be localized in the defect layers. This localization can be used to enhance the nonlinearity of PC if the defect layer is composed of nonlinear material. Expected field distribution should have the following features: strong localization of light in defect layer, which is useful for the lowering of requirements for the nonlinear coefficient of material and the intensity of input light; symmetric distribution of light in the two defects, which ensures that the refractive indices increments are the same, so the band-gap position of PC could be controlled more regularly.

Assuming that $S = N = 2$, when other parameters are the same as the ones in Fig. 2 and the frequency of input light is ω_0 , the field distribution of PC with the structure of $(AB)^S D(BA)^N B(AB)^N D(BA)^S$ is shown in Fig. 5, in which the horizontal axis represents the distance to x_0 ($x_0 = 0$) along the x -direction, and the vertical axis represents the normalized intensity of light. The normalized intensity in defect layers can also be called the localizing factor $G(x)$. To be seen clearly, the horizontal axis is divided into several segments to denote the layers of PC in Fig. 5, where the gray segments represent the defect layers. Though Fig. 5 shows that the light is localized, the field distribution in two defect layers is not symmetric, and $G(x)$ is not large enough to be applied. To get better results, the effects of material refractive indices on field distribution of PC are analyzed. When the other parameters are the same as the ones in Fig. 5, the effects of n_a and n_b are respectively shown in Fig. 6a and Fig. 6b. By comparing these figures, we can conclude that:

- i) When $n_a > n_b$, the localization of light in defect layers will be stronger if the difference value between n_a and n_b is larger.
- ii) With the varying n_a , field distribution in defect layers changes, and the ratio of the normalized intensity stays constant. Field distribution in defect layers changes with the varying n_b too, but the ratio of localization factors decreases with smaller n_b .

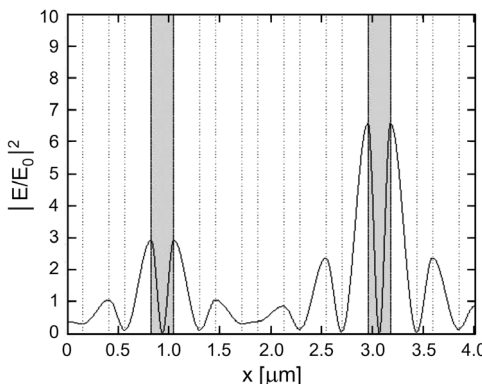


Fig. 5. Field distribution of 1D PC with dual-defects.

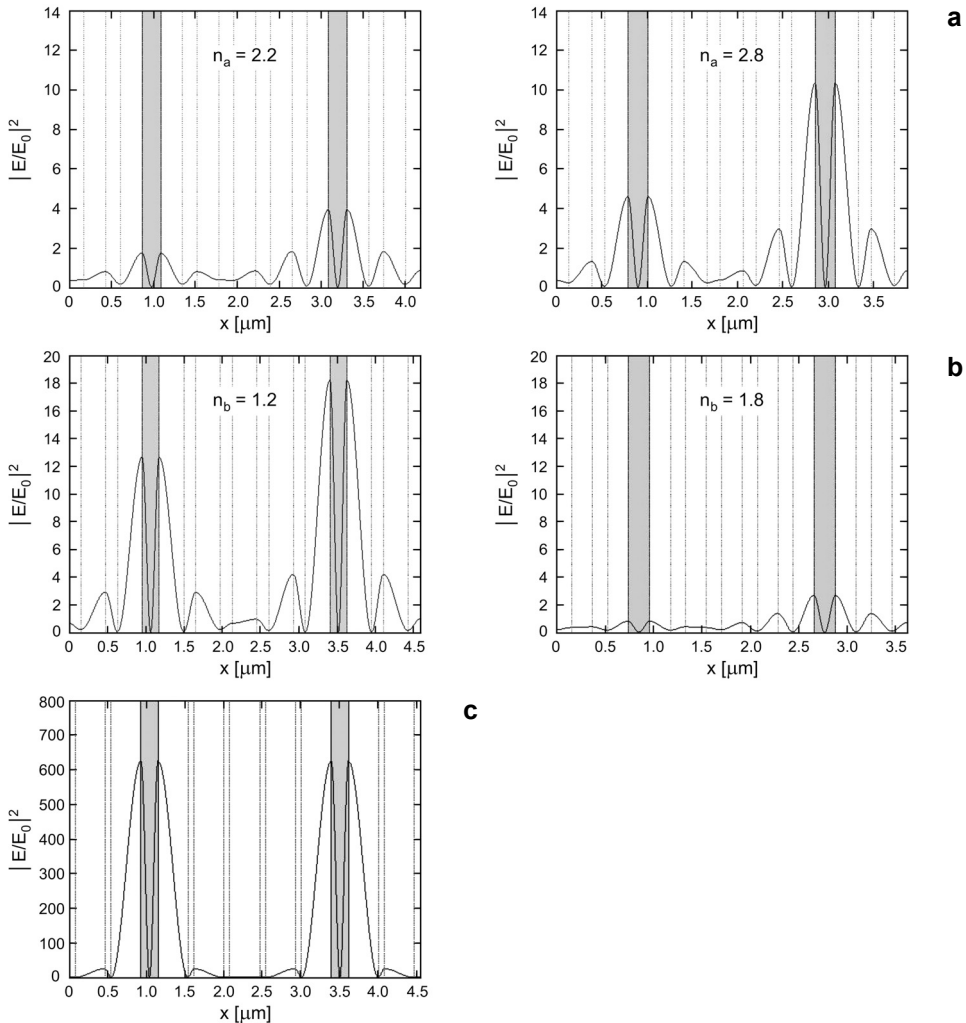


Fig. 6. Effects of material refractive indices on field distribution of 1D PC with dual-defects, (a) and (b) are corresponding to n_a and n_b , respectively, (c) shows the field distribution after optimization.

Our further studies indicate that this ratio will reduce to 1 if n_b is 1, which means that the symmetric field distribution is realized in the two defects.

According to the two conclusions above, symmetric field distribution with strong localization of light in the two defects can be realized by tuning material refractive indices, as shown in Fig. 6c, where n_a is 5.0, n_b is 1.0, the optical thicknesses of A and B are quarter-wavelength, the other parameters are the same as the ones in Fig. 5.

It should be pointed out that the bandwidth of BDM and the localization of the light in defects are on the mutual restrictive relationship by comparing the conclu-

sions in this section and the ones in the last section. This situation should be considered in related applications.

3.3. Stable control of nonlinear process

To use the strong localization, the defect layers in 1D PC are composed of Kerr nonlinear material, whose refractive index can be expressed as:

$$n_d(x) = n_{d0} + qI(x) = n_{d0} + qG(x)I_{in} \quad (9)$$

where n_{d0} is the linear part of the refractive index; q is the nonlinear optical coefficient related to $\chi^{(3)}$; $I(x)$, which is equal to the product of input light intensity I_{in} and localization factor $G(x)$, is the light intensity in defect layers. Because $G(x)$ varies with x , each defect layer is regarded as a combination of many sub-layers with the same thickness in actual calculation. $G(x)$ can be treated as a constant in each sub-layer if the number of sub-layers is large enough. Considering the results' precision and the time efficiency, we assumed that the number is 100.

In Section 1, we have mentioned that the nonlinear process in 1D PC with nonlinear defects is unstable. The reason can be concluded to the interaction between the refractive index of nonlinear material and the field distribution. On the one hand, the field distribution of light with the frequency of ω_0 in defect layers is sensitive to the refractive index of defects and the transmittance of PC at central frequency. Considering that the defects are composed of nonlinear material, when $n_d(x)$ varies with I_{in} , the field of light will be redistributed due to the change of $n_d(x)$ and the variation of transmittance at central frequency. On the other hand, $n_d(x)$ will change if $G(x)$ changes according to Eq. (9). Though strong localization can also be realized in traditional 1D PC with one defect, the bandwidth of the defect mode is pretty narrow, which means that the transmittance of PC at the frequency of defect mode will change a lot even if the shifting of the band-gap is tiny.

In the applications based on 1D PC with one nonlinear defect, the localization of light in defect layer is very strong before the refractive index of nonlinear material changes. However, when the changing happens, field distribution will change a lot and $G(x)$ will become very small due to the change of refractive index and especially the significant variation of PC's transmittance at the frequency. As a result, the difference value of refractive index decreases rapidly, and all the properties of PC nearly go back to their original states. This process will repeat multiple times. Thus it can be seen that because of the interaction between $n_d(x)$ and $G(x)$, the nonlinear process is unstable, which is not good for nonlinear PC to be applied and should be avoided.

BDM studied in Section 3.1. can be used to solve this problem. Before the refractive indices of nonlinear material changed, light localizations in the two defect layers are both very strong. After the changing of refractive indices, the central frequency ω_0 can still exist in the BDM probably. In this situation, the transmittance at ω_0 will have little change, adding that not only the absolute variation but also the relative variation of $n_d(x)$ is very small. (They are only of the order of 10^{-4} in the examples in this letter.)

$G(x)$ will have little change, too. Thus the filed distribution of PC after changing the nonlinear refractive indices is just the same as the one before the refractive indices changed, which means the nonlinear process is stable now with the help of BDM.

3.4. Realization of AOLG

According to the analysis of the last two sections, symmetric distribution and strong localization of the light can be realized in the two nonlinear defect layers in 1D PC with the structure of $(AB)^S D (BA)^N B (AB)^N D (BA)^S$. Meanwhile, the nonlinear process could be stable with the help of BDM. Having solved these two key problems mentioned in the introduction, to realize AOLG, we still need a frequency point at which the transmittances before and after the shifting of the band-gap are of high-contrast. This point can be gained by cascading two PC together. In this condition, two connected A can be regarded as a new defect, which leads to two narrow transmission peaks existing in the band-gap beside the BDM. Each one of the peaks can be chosen as the probe channel.

Expected AOLG can be realized based on the cascading structure. Parameters are as follows: period numbers S and N are both 2; refractive indices of A and B are 3.45

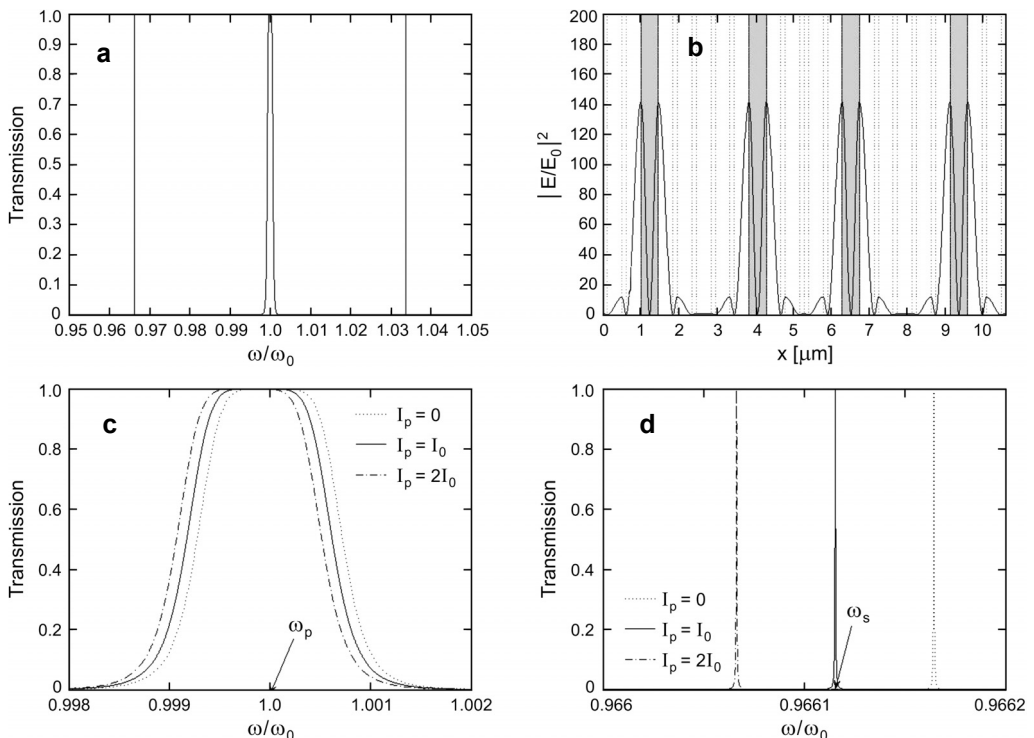


Fig. 7. Realization of AOLG. (a) and (b) shows the transmission spectrum and field distribution of the cascading 1D PC with dual-defects, respectively; (c) and (d) show the transmission spectrum near ω_0 and ω_s with different pump intensities.

and 1, which are the values of silicon and air, respectively, their thicknesses are determined by $a n_a = b n_b = \lambda_0/4$; D is composed of the nonlinear material CuCl, whose linear part of refractive index is $n_{d0} = 1.706$ and thickness is determined by $d = (\lambda_0/2)/n_{d0}$. CuCl not only has a large nonlinear coefficient $q = 3 \times 10^{-7} \text{ cm}^2/\text{kW}$ but also has a small corresponding time in femto-second area [9]; frequencies of two pump light beams P1 and P2 are $\omega_{p1} = \omega_{p2} = \omega_0$, and the intensities are I_{P1} and I_{P2} , respectively; frequency of probe light is near the narrow transmission peak $\omega_s = 0.966115\omega_0$, its intensity is I_s . We introduce a new parameter $I_0 = 10 \text{ kW/cm}^2$, which represents the light intensity of the digital signal 1.

When the intensities of incident pump light beams are both 0, transmission spectrum of PC and field distribution at the central frequency are shown in Figs. 7a and 7b, where the BDM, the narrow transmission peaks and the symmetric distributed field can be seen. The intensity of each beam is either 0 (logic signal 0) or I_0 (logic signal 1). These two beams can be regarded as just one incident light beam P, which has three logic states: 0, 1 and 2, and the corresponding intensities I_p are 0, I_0 and $2I_0$, respectively. Figures 7c and 7d show the transmission spectrum near ω_0 and ω_s with different pump intensities, where the dotted, solid and dot-dash lines are corresponding

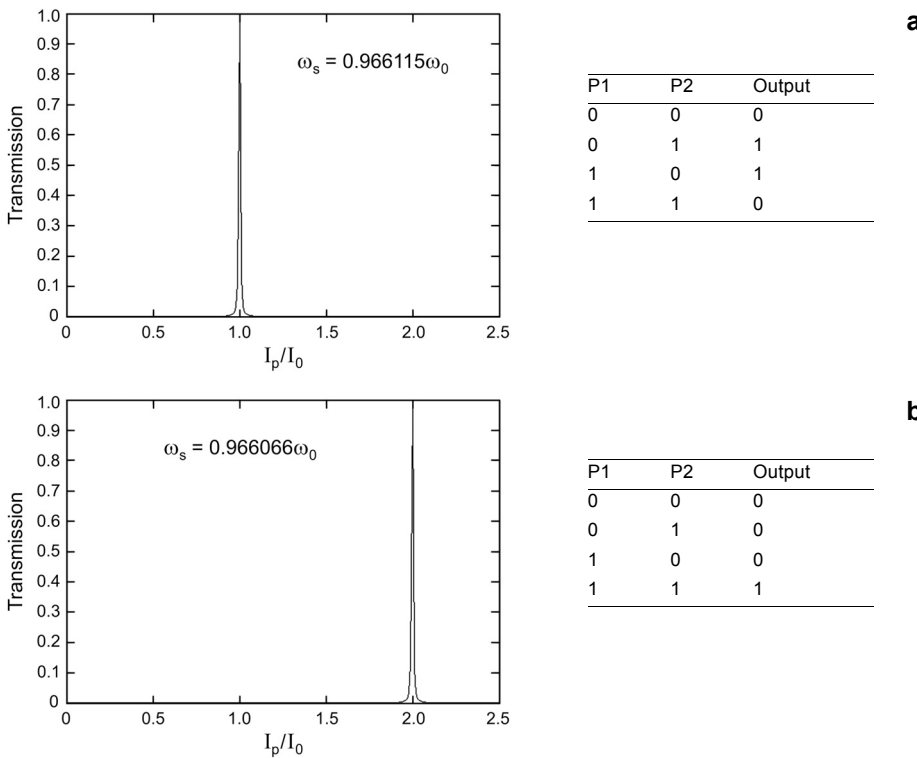


Fig. 8. Realization of AOLG. (a) and (b) are the simulation results and truth tables corresponding to XOR gate and AND gate, respectively.

to $I_p = 0$, $I_p = I_0$ and $I_p = 2I_0$, respectively. It can be seen that the pump lights are always located in BDM in the three situations, though the probe light is located in narrow transmission peak just when $I_p = I_0$. That is to say, the probe light cannot get through the PC (the logic output is 0) when the two pump light beams are both at the state of 0 or 1. Just when one of the beams is at the state of 0 while the other one is at the state of 1, the probe light can get through (the logic output is 1). So the function of XOR logic gates has been realized.

It can be seen in Fig. 7d that, because the transmission peak is very narrow, a little tiny shifting of the band-gap could lead to big change of transmittance at ω_s , which means that small deviations in refraction index of D-layers could lead to visible results. Meanwhile, the transmittance at ω_0 keeps the same due to the BDM. That is why we choose ω_0 as the frequency of the pump light and pick the transmission peak to filter the probe light.

Figure 8a clearly describes the realization of XOR logic gates from another perspective, where horizontal axis represents the normalized intensity of pump light beams, and vertical axis represents the transmittance of the probe light. With one of the pump light beams being set at the state of 1 permanently, the output state will be opposite to the state of the other one. That is the function of NOT gate. When the frequency of probe light is chosen properly, the PC can also be used as other logic gates. For example, AND gate can be realized with $\omega_s = 0.966066\omega_0$, because the probe light can get through the PC just when the states of two pump light beams are 1, as shown in Fig. 8b. It can also be seen in Fig. 8 that the transmittances of state 0 and 1 are of high-contrast, which is useful for the state decision of output signal.

4. Conclusions

In this letter, we proposed a resolution to realize nonlinearity-controllable all-optical logic gates based on 1D PC with dual defects. By studying the transmission spectrum and field distribution with the transfer matrix method, we developed the methods of realizing BDM near the central frequency, symmetrically distributed field and strong localization in the two defects. Finally, we used these methods to design XOR, NOT and AND AOLG, that have more advantages compared with traditional logic gates based on 1D PC with one defect as follows:

i) Low threshold. Then the intensity of the pump light is 3 orders lower than the one in [9] due to the light localization in defect layers. What is more, the threshold can be even lower by choosing material with larger refractive index to compose A.

ii) Stable control. The nonlinear process can be stably controlled by reducing the influence between the nonlinear refractive index and the field distribution with BDM, which could be used in other applications of nonlinear 1D PC.

iii) High contrast. Because we chose the narrow transmission peak as the probe light channel instead of the edge of band-gap, the ratio between the transmittances of

state 0 and 1 is much larger than the one in [8]. Based on these advantages, AOLG proposed in this letter is better while applying in all-optical signal processing.

Acknowledgements – This research was supported in part by NSFC (No. 60707001, No. 60711140087), National 973 Program (No. 2007CB310705), National 863 Program (No. 2007AA01Z2a6, No. 2009AA01Z214), NCET (07-0110), PCSIRT (No. IRT0609), ISTCP (No. 2006DFA11040), P.R. China.

References

- [1] RAMASWAMI R., *Multiwavelength lightwave networks for computer communication*, IEEE Communications Magazine **31**(2), 1993, pp. 78–88.
- [2] NIYAMA A., KOSHIBA M., *Three-dimensional beam propagation analysis of nonlinear optical fibers and optical logic gates*, Journal of Lightwave Technology **16**(1), 1998, pp. 162–168.
- [3] ZHAO C., ZHANG X.L., DONG J.J., HUANG D.X., *Investigation on all-optical logic AND and NOR gates based on the same structure*, Acta Physica Sinica **55**(8), 2006, pp. 4150–4155.
- [4] SHARAIHA A., TOPOMONDZO J., MOREL P., *All-optical logic AND–NOR gate with three inputs based on cross-gain modulation in a semiconductor optical amplifier*, Optics Communications **265**(1), 2006, pp. 322–325.
- [5] TIAN H.P., TIAN J.P., JI Y.F., *Bright and dark solitons in quadratic nonlinear periodic structures and application to an all-optical logic gates*, Journal of Physics B: Atomic, Molecular and Optical Physics **40**(7), 2007, pp. 1391–1402.
- [6] LAI D.M., KWOK C.H., WONG K.K., *All-optical picoseconds logic gates based on a fiber optical parametric amplifier*, Optics Express **16**(22), 2008, pp. 18362–18370.
- [7] YABLONOVITCH E., *Inhibited spontaneous emission in solid-state physics and electronics*, Physical Review Letters **58**(20), 1987, pp. 2059–2062.
- [8] SAJEEV J., *Strong localization of photons in certain disordered dielectric superlattices*, Physical Review Letters **58**(23), 1987, pp. 2486–2489.
- [9] NEFEDOV I., MOROZOV Y., *Optical controlling photonic band gap logic elements*, The second International Conference on Transparent Optical Networks, June 5–8, 2000, Gdańsk, Poland, pp. 195–198.
- [10] GLUSHKO E.YA., ZAKHIDOV A.A., *Theory of the nonlinear all-optical logic gates based on PBG structures*, The second International Conference on Advanced Optoelectronics and Lasers, September 12–17, 2005, Yalta, Crimea, Ukraine, pp. 184–190.
- [11] ZOU H., LIANG G.Q., WANG H.Z., *Efficient all-optical dual-channel switches, logic gates, half-adder, half-subtractor in a one-dimensional photonic heterostructure*, Journal of the Optical Society of America B **25**(3), 2008, pp. 351–360.
- [12] ZHU Z.H., YE W.M., JI J.R., YUAN X.D., ZEN C., *High-contrast light-by-light switching and AND gate based on nonlinear photonic crystals*, Optics Express **14**(5), 2006, pp. 1783–1788.
- [13] WANG H., LI Y.P., *An eigen matrix method for obtaining the band structure of photonic crystals*, Acta Physica Sinica **50**(11), 2001, pp. 2172–2178.
- [14] ZHOU Q.C., *Distribution of electrical field and density of electromagnetic mode in finite one-dimensional photonic crystal*, Journal of East China Shipbuilding Institute (Natural Science Edition) **19**(1), 2005, pp. 27–31.

Received April 9, 2009
in revised form November 21, 2009